IEEE Access
Multidisciplinary | Rapid Review | Open Access Journal

Received March 26, 2022, accepted April 18, 2022, date of publication April 22, 2022, date of current version May 5, 2022.

Digital Object Identifier 10.1109/ACCESS.2022.3169505

Sliding-Window Turbo Equalization and Its Reduced-Complexity Decoding Techniques

SIRAWIT KHITTIWITCHAYAKUL AND WATID PHAKPHISUT, (Member, IEEE)
School of Engineering, King Mongkut's Institute of Technology Ladkrabang, Bangkok 10520, Thailand
Corresponding author: Watid Phakphisut (watid.ph@kmitl.ac.th)

This work was supported by the National Science, Research and Innovation Fund (NSRF) under Contract RE-KRIS/FF65/33.

ABSTRACT Turbo equalization is a cooperative error-correcting approach to achieve a target bit-error rate over inter-symbol interference channels. In this paper, we proposed a new turbo equalization, called sliding-window turbo equalization (SW-TE), consisting of the Bahl-Cocke-Jelinek-Raviv detector and a spatially coupled, low-density, parity-check decoder. Moreover, the Protograph-based Extrinsic Information Transfer (P-EXIT) chart was modified to investigate the asymptotic behavior of SW-TE. Our analyses showed that SW-TE outperformed conventional turbo equalization in terms of decoding threshold. Based on the P-EXIT chart analysis, we further proposed a guideline of the reduced-complexity decoding techniques for SW-TE, eliminating unnecessary branch metric updates during turbo iterative decoding. Our simulations corroborated the analytical results, showing that SW-TE outperformed conventional turbo equalization while maintaining an acceptable level of complexity.

INDEX TERMS SC-LDPC codes, sliding window decoding, turbo equalization, P-EXIT chart.

I. INTRODUCTION

Inter-symbol interference (ISI) affects data integrity in high-rate digital communication [1] and high-density data storage systems [2]. Turbo equalization [3], [4] has been presented as an error-correcting approach to retrieve the original data in such ISI applications. The main idea behind turbo equalization is to treat the ISI channel as an inner code, serially concatenated to an error-correcting code as an outer code. To deal with them, Alhussien *et al.* [5] and Sun *et al.* [6] presented iterative soft-input soft-output (SISO) decoding between an inner detector and an outer decoder, allowing ISI to be overcome. The iterative decoding that includes both the inner detector and the outer decoder is referred to as turbo equalization. Until now, turbo equalization presented the research problem of choosing the most suitable outer code and decoder for various ISI applications [7]–[9].

Among existing error-correcting codes, spatially coupled LDPC (SC-LDPC) codes [10] have been shown to achieve the maximum a-posteriori (MAP) thresholds of the underlying LDPC codes [11]. Pusane *et al.* [12] and Hassan *et al.* [13] also showed that the SC-LDPC decoder with a sum-product algorithm [14] enabled significant performance gains over underlying LDPC codes. Moreover, SC-LDPC codes support sliding window decoding [15], which limits the latency and complexity of the SC-LDPC decoder. There has recently been a lot of research into message-passing algorithms to improve the SC-LDPC window decoder. Ali *et al.* [16] modified sum-product algorithms to mitigate error propagation, and Klaiber *et al.* [17] proposed their adaptive iterations to avoid burst-like error patterns. In addition, Hassan *et al.* [18] designed the sum-product algorithm's stopping conditions based on soft bit-error rate (BER) indicator to reduce window decoding complexity.

Over the last five years, SC-LDPC codes have emerged as an excellent outer code for ISI applications, such as magnetic recording systems [19]–[24]. In [19], Esfahanizadeh *et al.* used SC-LDPC codes as the outer code in magnetic recording systems, and the Bahl-Cocke-Jelinek-Raviv (BCJR) [25] as the inner detector. The structure of the SC-LDPC codes was then designed to match the characteristics of the output signal of BCJR. SC-LDPC codes are still used as an outer code by Yang *et al.* [20], and their structures are designed for magnetic recording systems with additional ISI from adjacent tracks, such as two-dimensional (TDMR) magnetic recording systems. The designs [19]–[20] show BER improvements when compared to undesigned SC-LDPC codes and/or their underlying LDPC codes. Recently, Hareedy *et al.* designed circulant-based SC-LDPC codes for magnetic recording systems and introduced the concepts of various graph

The associate editor coordinating the review of this manuscript and approving it for publication was Pietro Savazzi.

patterns [21]. Furthermore, they extended [21] by constructing high-performance multi-dimensional SC-LDPC codes [22], which could mitigate many types of ISI and channel non-uniformity in magnetic recording systems.

Previous works [19]–[22] have only focused on SC-LDPC codes with complete block decoding. Therefore, in our previous work [23], SC-LDPC codes with window decoding were used in bit pattern-media magnetic recording (BPMR) systems for the first time, allowing decoding latency and complexity to be independent of codeword length. Moreover, dynamic window shifting was introduced to reduce the complexity of SC-LDPC decoding. Additional research of SC-LDPC codes with window decoding is considered in the turbo equalization of BPMR systems, as discussed in [24].

Based on the literature review, there is room to improve the performance of turbo equalization by modifying the message passing between the BCJR detector and SC-LDPC decoder. The first part of this paper is motivated by the fact that only the SC-LDPC decoder in turbo equalization uses window decoding, whereas the BCJR detector still produces messages with a complete block ensemble [23], [24]. In other words, the BCJR detector can only start processing when the SC-LDPC decoder has decoded all codewords, even though the SC-LDPC window decoder produces output nodes one by one. To be more consistent, we propose a new "sliding-window turbo equalization (SW-TE)" in which both the BCJR detector and the SC-LDPC decoder use window decoding (incorporating our conference version with preliminary results [26]). Our SW-TE can be viewed as the iterative message-passing schedules of the BCJR detector and SC-LDPC decoder within a window, in which recent output information generated at any decoding position is used at subsequent positions by sliding a window. To investigate the performance of SW-TE, the Protograph-based Extrinsic Information Transfer (P-EXIT) chart [27] is modified to analyze the asymptotic behavior, i.e., decoding threshold. Our analyses show that the decoding thresholds of SW-TE are superior to conventional turbo equalization, but at the cost of increased complexity.

In the second part of this paper, we propose three reduced-complexity decoding techniques for the SW-TE based on mutual information tracking from the P-EXIT chart. The first technique, called irregular-updating, reduces branch metric computations when the associated variable nodes show mutual information saturation. In the second technique, we apply our dynamic-shifting technique [23], which allows the window to be shifted dynamically in multiple positions to reduce the number of unnecessary decoding positions. Unlike previous work [23], we use mutual information instead of BER estimation to design a dynamic shifting of the window. The third technique combines the irregular-updating and dynamic-shifting techniques. Our simulations corroborate our analytical results, showing that the complexity of SW-TE can be reduced by more than a factor of two without BER losses.

The major contributions of this paper can be summarized in the following three aspects:

- It presents a new turbo equalization called "SW-TE." Here, the SC-LDPC decoder and BCJR detector work together to perform iterative message-passing decoding within a window decoder. Then, the updated LLRs of the SC-LDPC decoder at any decoding position are used immediately (as initial values) to update the BCJR detector at the next positions by sliding a window.
- The P-EXIT chart [27] is modified to investigate asymptotic behavior, i.e., the decoding threshold of SW-TE. Our analyses show that the decoding thresholds of SW-TE improve as the numbers of turbo iterations ($Iter_{\mathrm{TURBO}}$) and window size (W) grow and are better than those of conventional turbo equalization.
- Three decoding techniques comprising 1) irregular-updating, 2) dynamic-shifting, and 3) their combination, are proposed to reduce the complexity of the SW-TE. The P-EXIT chart analysis helps in choosing the optimal updating and shifting factors, intending to minimize the number of updates while preserving original performance. Our simulations corroborate our analytical results, showing that the proposed techniques reduce SW-TE complexity by more than a factor of two while maintaining good BERs.

II. SPATIALLY COUPLED LDPC (SC-LDPC) CODES IN TURBO EQUALIZATION

A. PROTOGRAPH-BASED SC-LDPC CODES

This paper focuses on the LDPC codes constructed from a protograph [28] and base matrix ($\mathbf{B}_t$). Let $\mathbf{B} = [\mathbf{B}_1, \mathbf{B}_2, \ldots, \mathbf{B}_t, \ldots, \mathbf{B}_L]$ be the base matrices of the LDPC codes at time t, where $\mathbf{B}_t$ has n_{v} rows corresponding to the variable nodes, and n_{c} columns correspond to the check nodes of a protograph. For constructing the SC-LDPC code following Mitchell *et al.* [29], the edges of the variable node at time, t, will be connected to the check nodes at time, $t+k$, where $k = 0, 1, \ldots, m_{\mathrm{cc}}$. The memory, m_{cc}, defines the largest distance between coupled protographs. Due to the edge spreading, the matrix, $\mathbf{B}_t$, must be partitioned into component matrices, $\mathbf{B}_{k,t}$, which each must satisfy the condition, $\sum_{k=0}^{m_{cc}} \mathbf{B}_{k,t} = \mathbf{B}_t$. Hence, the matrix, $\mathbf{B}$, of SC-LDPC codes has a diagonal stair-like structure,

$$\mathbf{B} = \begin{bmatrix} \mathbf{B}_{0,1} & & & & & & & \\ \mathbf{B}_{1,1} & \mathbf{B}_{0,2} & & & & & & \\ \vdots & \mathbf{B}_{1,2} & \ddots & & & & & \\ \mathbf{B}_{m_{\mathrm{cc}},1} & \vdots & & \mathbf{B}_{0,t} & & & & \\ & \mathbf{B}_{m_{\mathrm{cc}},2} & & \mathbf{B}_{1,t} & \ddots & & & \\ & & \ddots & \vdots & & \mathbf{B}_{0,L} & & \\ & & & \mathbf{B}_{m_{\mathrm{cc}},t} & & \mathbf{B}_{1,L} & & \\ & & & & \ddots & \vdots & & \\ & & & & & \mathbf{B}_{m_{\mathrm{cc}},L} & & \end{bmatrix}. \quad (1)$$

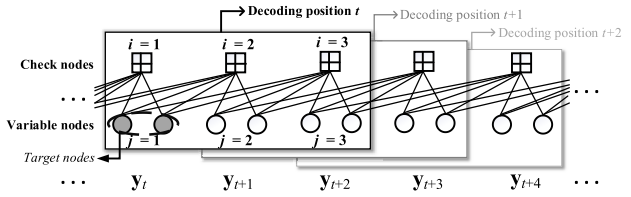

FIGURE 1. Illustration of window decoding with $W = 3$. The medium-rate SC-LDPC code is considered, by which $\mathbf{B}_{0,t} = \mathbf{B}_{1,t} = \mathbf{B}_{2,t} = [1\ 1]$.

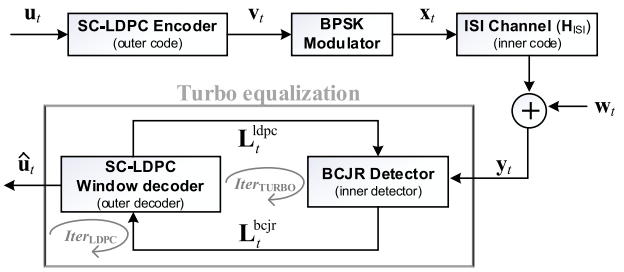

FIGURE 2. Block diagram of the channel model.

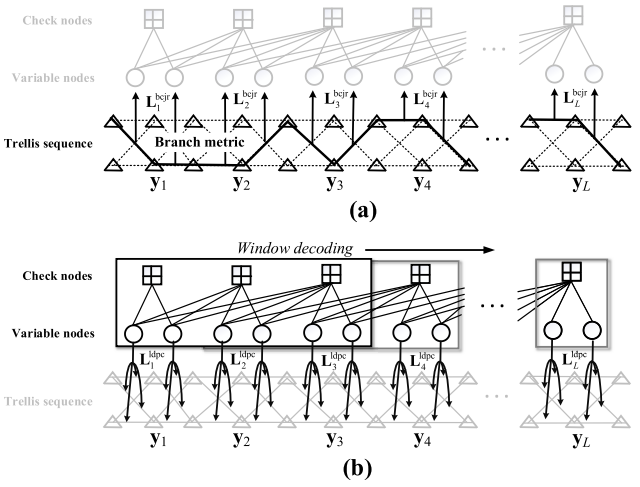

FIGURE 3. Illustration of LLR exchanges in the C-TE among (a) BCJR detection, and (b) SC-LDPC decoding.

An example of protograph's edge spreading with $\mathbf{B}_t = [3\ 3]$ and $m_{\text{cc}} = 2$, is the component matrices, $\mathbf{B}_{0,t} = \mathbf{B}_{1,t} = \mathbf{B}_{2,t} = [1\ 1]$. The parity-check matrix, $\mathbf{H}$, is obtained by replacing the non-zero elements of $\mathbf{B}$ by the $N \times N$ permutation matrix, and zero elements with the $N \times N$ zero matrix [30].

In the rest of this paper, we restrict our consideration to the medium-rate SC-LDPC code ($R = 0.490$) with $\mathbf{B}_{0,t} = \mathbf{B}_{1,t} = \mathbf{B}_{2,t} = [1\ 1]$, and high-rate SC-LDPC codes ($R = 0.796$) with $\mathbf{B}_{0,t} = \mathbf{B}_{1,t} = \mathbf{B}_{2,t} = [1\ 1\ 1\ 1\ 1]$. The coupling length is $L = 100$.

B. WINDOW DECODING

Decoding long codewords may require a large amount of memory, leading to high latency and complexity. Since the matrix, $\mathbf{B}$ in (1), has a diagonal band of non-zero entries, the SC-LDPC codes can use the window decoding [15] of size $W \geq m_{\text{cc}} + 1$. Fig. 1 illustrates the window decoder with $W = 3$. At each position t, the window decoder obtains the received signals, $\mathbf{y} = [\mathbf{y}_t, \mathbf{y}_{t+1} \ldots, \mathbf{y}_{t+W-1}]$, from a channel. In terms of the log-likelihood ratio (LLR), the soft information is produced and passed between the variable and check nodes within a window until the maximum number of decoding iterations ($Iter_{\text{LDPC}}$) is reached. Subsequently, the window decoder releases target nodes, $\mathbf{y}_t$, and shifts to the next position, $t = t + 1$, until $t = L$.

C. CONVENTIONAL TURBO EQUALIZATION (C-TE)

The block diagram in Fig. 2 depicts the channel model considered in this paper. On the transmitter side, the SC-LDPC encoder maps information block, $\mathbf{u}_t$, to the codeword block, $\mathbf{v}_t$. Subsequently, $\mathbf{v}_t$, is modulated to obtain the transmitted block, $\mathbf{x}_t = 2\mathbf{v}_t - 1$. Let $\mathbf{y}_t = [y_1, y_2, \ldots, y_n, \ldots, y_{n_{\text{v}}N}]$ be the received block, where the received, y_n, is expressed as,

$$y_n = \sum_{d=0}^{D-1} h_d x_{n-d} + w_n, \tag{2}$$

where $\mathbf{H}_{\text{ISI}} = [h_0, h_1, \ldots, h_m, \ldots, h_{D-1}]$ denotes an ISI coefficient matrix and $\mathbf{w}_t = [w_1, w_2, \ldots, w_n, \ldots, w_{n_{\text{v}}N}]$ is the Additive white Gaussian noise (AWGN) sequence.

In the rest of this paper, we consider the low ISI effect with $\mathbf{H}_{\text{ISI}} = [1\ \ 1]$, referred to as the PR1 channel, and the stronger ISI effect with $\mathbf{H}_{\text{ISI}} = [1\ \ 2\ \ 1]$, referred to as the PR2 channel. At the receiver side, the code blocks, $\mathbf{y} = [\mathbf{y}_1, \mathbf{y}_2, \ldots, \mathbf{y}_t, \ldots, \mathbf{y}_L]$, are passed to the turbo equalization.

Previous work [19]–[24] used the C-TE, which replaces traditional LDPC codes with SC-LDPC codes. Fig. 3 shows the LLR exchanges in the C-TE, with black lines denoting active edges and grey lines denoting inactive edges. As shown in Fig. 3(a), the BCJR detector [25] uses forward-backward algorithm to compute branch matrices (black dashed edges) and then selects the best surviving path (black solid edges). The LLRs, $\left[\mathbf{L}_1^{\text{bcjr}}, \mathbf{L}_2^{\text{bcjr}}, \ldots, \mathbf{L}_t^{\text{bcjr}}, \ldots, \mathbf{L}_L^{\text{bcjr}}\right]$, of each trellis section, involved in a surviving path, are produced, and passed to the SC-LDPC decoder. SC-LDPC decoding is performed using either the block method [19]–[22] or the sliding window method [23], [24]. Note that we consider the C-TE in this paper, in which the SC-LDPC decoder only uses window decoding [23], [24], as shown in Fig. 3(b). Then, LLRs, $\left[\mathbf{L}_1^{\text{ldpc}}, \mathbf{L}_2^{\text{ldpc}}, \ldots, \mathbf{L}_t^{\text{ldpc}}, \ldots, \mathbf{L}_L^{\text{ldpc}}\right]$, of all the variable nodes are produced by the sum-product algorithm [14] and passed back to update the branch matrices of the BCJR detector. The same process continues for the maximum number of turbo iterations ($Iter_{\text{TURBO}}$).

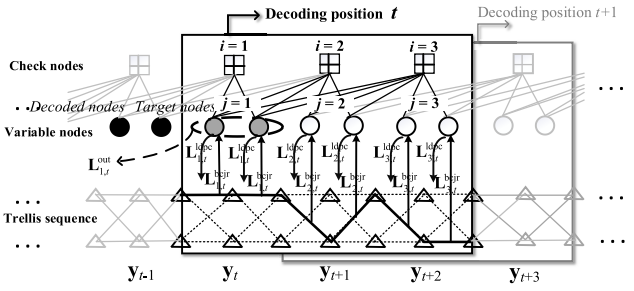

FIGURE 4. Illustration of the LLR exchanges in the SW-TE, $W = 3$.

III. PROPOSED TURBO EQUALIZATION

A. SLIDING-WINDOW TURBO EQUALIZATION (SW-TE)

In the C-TE, although the SC-LDPC decoder uses window decoding to release the output nodes one by one, the BCJR detector does not start processing until SC-LDPC decoder has decoded all variable nodes. Moreover, the BCJR detector requires the storage of the branch matrices on the total L consecutive trellis sections, which consumes a significant amount of memory [31], as discussed in Section III-B-2.

Based on the preceding discussion, we propose a new "SW-TE" that uses sliding-window processing to execute both the BCJR detector and SC-LDPC decoder. The iterative message-passing schedules for the BCJR detector and SC-LDPC decoder will be restricted within a window size, W.

Let j be the index of the variable node at position t. During the iterative message-passing procedure, the BCJR detector produces $\mathbf{L}_{j,t}^{\text{bcjr}}$ from the surviving path to the variable node, j. Then, the SC-LDPC decoder produces $\mathbf{L}_{j,t}^{\text{ldpc}}$ back to update the branch metrics. Fig. 4 depicts LLR exchanges in the SW-TE with $W = 3$, with black lines denoting active edges and grey lines denoting inactive edges. At decoding position t, the BCJR detector produces $\left[\mathbf{L}_{1,t}^{\text{bcjr}}\ \mathbf{L}_{2,t}^{\text{bcjr}}\ \mathbf{L}_{3,t}^{\text{bcjr}}\right]$ from their surviving path and passes it to the SC-LDPC decoder. Subsequently, the SC-LDPC decoder produces $\left[\mathbf{L}_{1,t}^{\text{ldpc}}\ \mathbf{L}_{2,t}^{\text{ldpc}}\ \mathbf{L}_{3,t}^{\text{ldpc}}\right]$ and passes it back to update the branch matrices of the BCJR detector. The same process is repeated for $Iter_{\text{TURBO}}$, and the target node, $\mathbf{v}_t$, is decided based on the output LLR, $\mathbf{L}_{1,t}^{\text{out}}$. The window then shifts to the next position, $t = t + 1$, until $t = L$.

B. IMPLEMENTATION COMPLEXITY

In this part, we discuss some implementation complexities of the SW-TE in a variety the ISI channel.

1) NUMBER OF UPDATES

The number of updates [18], [23] (also called the number of effective iterations in some studies [32]) is one of the criteria used to evaluate the implementation complexity. This value can imply how long it takes to decode the codewords, which is necessary to keep in mind in high-speed applications. In this part, we evaluate the number of updates required to complete one output node ($U_{\text{1-node}}$). Given that $U_{\text{1-node}}^{\text{bcjr}}$ is the number of branch metric updates in the BCJR detector:

$$U_{\text{1-node}}^{\text{bm}} = \frac{1}{L} \sum_{r=1}^{Iter_{\text{TURBO}}} \sum_{t=1}^{L} N_{r,t}^{\text{bm}}, \tag{3}$$

where $N_{r,t}^{\text{bm}}$ is the number of branch metrics updated at time t, and turbo iteration r.

Moreover, we define $U_{\text{1-node}}^{\text{ve}}$ as the number of variable node edge updates in the SC-LDPC decoder:

$$U_{\text{1-node}}^{\text{ve}} = \frac{1}{L} \sum_{r=1}^{Iter_{\text{TURBO}}} \sum_{t=1}^{L} N_{r,t}^{\text{ve}}, \tag{4}$$

where $N_{r,t}^{\text{ve}}$ is the number of edges updated at time t, and turbo iteration r. The resulting number of updates (3) - (4) for the SW-TE and C-TE will be discussed in detail in Section IV-C-3.

It should be noted this paper did not include the number of check node edge updates because it is directly proportional to the number of variable node edge updates.

2) MEMORY REQUIREMENTS

In this part, we evaluate the implementation complexity in terms of the memory requirements. According to Bahl *et al.*'s work [25], branch matrices of the BCJR detector are generated on the consecutive trellis sections. For our SW-TE, the BCJR detector generates branch matrices on the W trellis sections only. As a result, the memory required to store all the branch metrics is: $M^{\text{bm}} = 2^{D+1}W$, where D is the length of the ISI coefficient matrix. Unlike the SW-TE, the BCJR detector in previous C-TE [23], [24] generates branch matrices for the total length of L trellis sections, resulting in $M^{\text{bm}} = 2^{D+1}L$. Thus, our SW-TE has a lower M^{bm} than C-TE for every channel and code parameter because of $W < L$. Note that synchronized forward-backward algorithms [33] can be used to further reduce M^{bm} in the BCJR detector of the C-TE and SW-TE.

For the SC-LDPC decoder, we need a storage element for every variable node edge in the protograph [34]. In addition, each variable node also needs a storage element for incoming LLRs from the BCJR detector. Therefore, each variable node requires $d_{\text{v}} + 1$ storage elements per iteration, where d_{v} is the number of variable node edges. As a result, the memory requirement of SC-LDPC window decoding for completing $Iter_{\text{LDPC}}$ is $M^{\text{ve}} = WIter_{\text{LDPC}}(d_{\text{v}} + 1)$, which is independent of the codeword length L. There is no difference between the C-TE and the SW-TE in terms of M^{ve} because they both use sliding-window processing for the SC-LDPC decoder.

IV. THEORETICAL ANALYSIS OF TURBO EQUALIZATIONS IN ISI CHANNEL

The P-EXIT chart [27] introduces mutual information tracking the edges of the protograph. In this section, the P-EXIT chart is modified to analyze mutual information exchanges in

the C-TE and SW-TE. Moreover, asymptotic behavior, i.e., decoding threshold and number of updates, is also presented.

A. P-EXIT CHART ANALYSIS FOR C-TE

Let $1 \leq r \leq Iter_{\text{TURBO}}$ be the turbo iteration index, and $1 \leq l \leq Iter_{\text{LDPC}}$ be the decoding iteration index. We define the index, i, as the position of the check node, and j as the position of the variable node at decoding position t. The element, b_{ij}, is the number of edges connected to the check node, i, and variable node, j. The first step in the P-EXIT chart for turbo equalization (also called turbo-like P-EXIT chart) is to initialize the signal-to-noise ratio (E_b/N_0) and code rate (R) [35]. **Steps 1)–10)** of the P-EXIT chart for the C-TE are as follows:

1) Initialize E_b/N_0 and R.
   Set $r = 1$.
2) Compute the a posteriori mutual information, $I^{Ed}(r)$, from the BCJR detector's output LLRs, as obtained by the Monte Carlo simulation [35] for the given E_b/N_0, R, and a priori mutual information, $I^{Ad}(r-1)$.
   Note that $I^{Ad}(0) = 0$.
3) Set $t = 1$ and $l = 1$.
4) Compute the mutual information, $I^{Ev}_{j\to i}(r,l)$, from the variable node, j, to check node, i,

$$I^{Ev}_{j\to i,t}(r,l) = J\left(\sqrt{\sum_{s=1}^{W}(b_{sj}-\tau)\left(J^{-1}\left(I^{Ec}_{s\to j,t}(l-1)\right)\right)^2 + \left(J^{-1}\left(I^{Ed}(r)\right)\right)^2}\right), \tag{5}$$

   where $\tau = 1$ if $s = i$ and $\tau = 0$ if $s \neq i$. The polynomial approximations, $J(\cdot)$, of the mutual information and its inverse function, $J^{-1}(\cdot)$, are given in [36].
5) Compute the mutual information, $I^{Ec}_{i\to j,t}(r,l)$, from the check node, i, to variable node, j,

$$I^{Ec}_{i\to j,t}(r,l) = 1 - J\left(\sqrt{\sum_{s=1}^{W}(b_{is}-\tau)\left(J^{-1}\left(1-I^{Ev}_{s\to i,t}(l)\right)\right)^2 + \sum_{k=1}^{m_{cc}} b_{i+k,1}\left(J^{-1}\left(1-I^{Ev}_{1\to i+k,t-k}(Iter_{\text{LDPC}})\right)\right)^2}\right), \tag{6}$$

   where $\tau = 1$ if $s = j$ and $\tau = 0$ if $s \neq j$.
6) Compute the cumulative mutual information, $I^{Cm}_{j,t}(r,l)$, and a priori mutual information $I^{Ad}_{j,t}(r,l)$,

$$I^{Cm}_{j,t}(r,l) = J\left(\sqrt{\sum_{i=1}^{W} b_{ij}\left(J^{-1}\left(I^{Ec}_{i\to j,t}(l)\right)\right)^2 + \left(J^{-1}\left(I^{Ed}(r)\right)\right)^2}\right), \tag{7}$$

$$I^{Ad}_{j,t}(r,l) = J\left(\sqrt{\sum_{i=1}^{W} b_{ij}\left(J^{-1}\left(I^{Ec}_{i\to j,t}(l)\right)\right)^2}\right). \tag{8}$$

7) Increase $l = l + 1$.
   Repeat **steps 4) – 7)** until $l > Iter_{\text{LDPC}}$.
8) Shift the window to the next position, $t = t + 1$.
   Reset $l = 1$ and repeat **steps 4) – 8)** until $t > L$.
9) Compute averaged a priori mutual information $I^{Ad}_{avg}(r)$,

$$I^{Ad}_{avg}(r) = \frac{1}{L}\sum_{t=1}^{L} I^{Ad}_{1,t}(r, Iter_{\text{LDPC}}). \tag{9}$$

10) Set $I^{Ad}(r) = I^{Ad}_{avg}(r)$.
    Increase $r = r + 1$.
    Repeat **steps 2) – 10)** until $I^{Cm}_{1,t}(r,l) \to 1$ for all decoding positions, t, or $r > Iter_{\text{TURBO}}$.

In this paper, the numerical value, "decoding threshold," is used to refer to the lowest channel quantity that ensures no error after decoding. We calculate the decoding threshold of the C-TE (and SW-TE) from the lowest E_b/N_0 (dB) that provide $I^{Cm}_{1,t}(r,l) \to 1, \forall t$.

B. P-EXIT CHART ANALYSIS FOR SW-TE

In the C-TE, the BCJR detector starts to process only after receiving the LLRs from all variable nodes. Therefore, the identical (averaged) mutual information, $I^{Ad}_{avg}(r)$ in (9), can represent a priori mutual information for all variable nodes, which is passed back to the BCJR detector. Our SW-TE, unlike the C-TE, only considers branch metrics and variable nodes within a window. Hence, a priori mutual information of each variable node, j, may differ; as a result, we use $I^{Ad}_{j,t}(r)$ to present a priori mutual information of the variable node, j, at position t. The P-EXIT chart for the SW-TE can be summarized in **steps 1) – 8)** as follows:

1) Initialize E_b/N_0 and R.
   Set $t = 1$, $r = 1$, and $l = 1$.
2) Compute the a posteriori mutual information, $I^{Ed}_{j,t}(r)$, by the Monte Carlo simulation [35] for given E_b/N_0, R, and a priori mutual information $I^{Ad}_{j,t}(r-1)$.
   Note that,

$$I^{Ad}_{j,t}(0) = \begin{cases} I^{Ad}_{j+1,t-1}(Iter_{\text{TURBO}}), & \text{if } t \geq 2 \text{ and } j \leq W-1 \\ 0, & \text{otherwise} \end{cases}$$

3) Compute the mutual information, $I^{Ev}_{j\to i}(r,l)$ by

$$I^{Ev}_{j\to i,t}(r,l) = J\left(\sqrt{\sum_{s=1}^{W}(b_{sj}-\tau)\left(J^{-1}\left(I^{Ec}_{s\to j,t}(l-1)\right)\right)^2 + \left(J^{-1}\left(I^{Ed}_{j,t}(r)\right)\right)^2}\right), \tag{10}$$

4) Compute the mutual information, $I^{Ec}_{i\to j,t}(r,l)$, via (6).
5) Compute the mutual information, $I^{Cm}_{j,t}(l)$,

$$I^{Cm}_{j,t}(r,l) = J\left(\sqrt{\sum_{i=1}^{W} b_{ij}\left(J^{-1}\left(I^{Ec}_{i\to j,t}(l)\right)\right)^2 + \left(J^{-1}\left(I^{Ed}_{j,t}(r)\right)\right)^2}\right), \tag{11}$$

and a priori mutual information $I^{Ad}_{j,t}(r,l)$ via (8).
6) Increase $l = l+1$.
Repeat **steps 3) – 6)** until $l > Iter_{\text{LDPC}}$.
7) Set $I^{Ad}_{j,t}(r) = I^{Ad}_{j,t}(r, Iter_{\text{LDPC}})$.
Increase $r = r+1$.
Reset $l = 1$ and repeat **steps 2) – 7)** until $r > Iter_{\text{TURBO}}$.
8) Shift the window to the next position, $t = t+1$.
Reset $r = 1$ and repeat **steps 2) – 8)** until $t > L$.

C. ANALYTICAL RESULTS VIA P-EXIT CHARTS

1) MEDIUM-RATE SC-LDPC CODES

This part investigates the decoding thresholds of the C-TE and SW-TE when using medium-rate SC-LDPC codes. Fig. 5 compares the decoding thresholds for C-TE and SW-TE, with turbo iteration numbers ($Iter_{\text{TURBO}}$) ranging from 1 to 10. The window size is $W = 10$. Our investigation begins with the PR1 channel –see in circle symbols. The results show that, as $Iter_{\text{TURBO}}$ increases, the decoding thresholds for both C-TE and SW-TE decrease (improve) until $Iter_{\text{TURBO}}$ reaches 6. For every $Iter_{\text{TURBO}}$, the decoding thresholds of the SW-TE are lower (better) than that of the C-TE. For example, the SW-TE improves the decoding threshold by about 0.43 dB at $Iter_{\text{TURBO}} = 6$. The curves for the PR2 channel are similar to those for the PR1, with increasing $Iter_{\text{TURBO}}$ improving the decoding threshold (see square symbols). The SW-TE has about 0.87 dB lower decoding threshold than the C-TE at $Iter_{\text{TURBO}} = 6$.

In Fig. 6, the decoding threshold is plotted against the window size (W), with $Iter_{\text{TURBO}}$ set to 6. The decoding thresholds of C-TE and SW-TE diminish as W increases for the PR1 channel, though they stop decreasing at $W \geq 10$. We found that the decoding thresholds of SW-TE are lower than that of the C-TE by about 0.43 dB at $W = 10$. The SW-TE outperforms the C-TE on the PR2 channel, where their decoding thresholds are about 0.87 dB lower.

Based on the results in Figs. 5 - 6, the C-TE and SW-TE converge to the same point of turbo iteration ($Iter_{\text{TURBO}} \geq 6$) and window size ($W \geq 10$). These results serve as guidelines for determining the lowest channel quality and required coding parameters for C-TE and SW-TE.

2) HIGH-RATE SC-LDPC CODES

Investigations of the C-TE and SW-TE when using high-rate SC-LDPC codes are shown in this part. Fig. 7 shows the relationship between the decoding threshold and $Iter_{\text{TURBO}}$. Similar to the medium-rate case, the decoding thresholds of

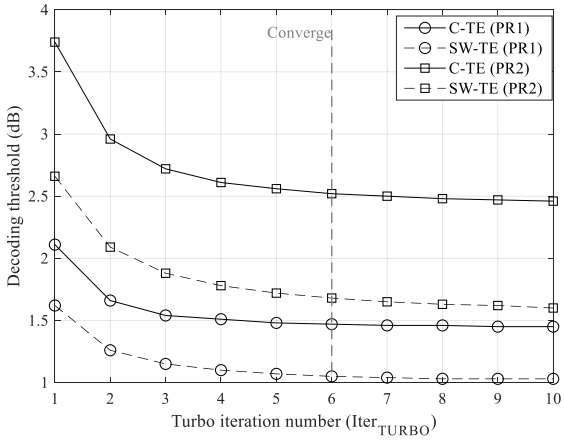

FIGURE 5. Relationship between decoding threshold and turbo iteration. The medium-rate SC-LDPC codes are considered by $\mathbf{B}_{0,t} = \mathbf{B}_{1,t} = \mathbf{B}_{2,t} = [1\ 1]$.

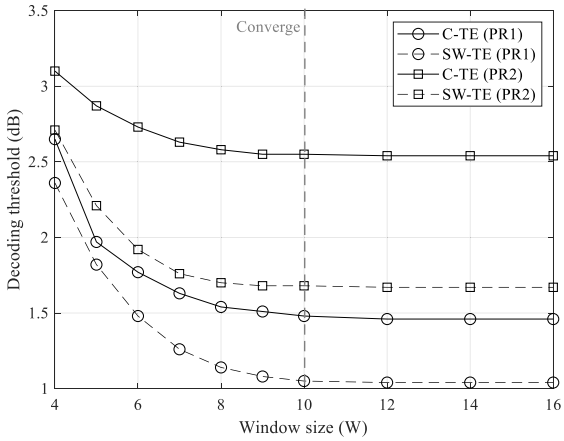

FIGURE 6. Relationship between decoding threshold and window size. The medium-rate SC-LDPC codes are considered by $\mathbf{B}_{0,t} = \mathbf{B}_{1,t} = \mathbf{B}_{2,t} = [1\ 1]$.

C-TE and SW-TE decrease by increasing $Iter_{\text{TURBO}}$ and converge at $Iter_{\text{TURBO}} = 6$ for both the PR1 and PR2 channels. The decoding thresholds of the SW-TE are still lower than that of the C-TE for every $Iter_{\text{TURBO}}$.

Window size (W) still affects the decoding threshold, as seen in Fig. 8, with a larger W decreasing the decoding threshold. It is important to note that the decoding thresholds for the PR2 channel decrease slightly as W increases. The results also show that decoding thresholds converge at $W = 8$, with the SW-TE decoding thresholds remaining lower than the C-TE for every W.

3) COMPARISONS OF NUMBER OF UPDATES

In this part, we restrict our consideration to compare the number of updates, $U^{\text{bm/ve}}_{\text{1-node}}$ (3) – (4), between the C-TE and the SW-TE. We set $Iter_{\text{TURBO}} = 6$ and W ranges from 4 to 16. Fig. 9 (upper) shows that $U^{\text{bm}}_{\text{1-node}}$ the C-TE remains constant, whereas the SW-TE grows rapidly as W increases. This comes from the fact that the SW-TE uses sliding-window

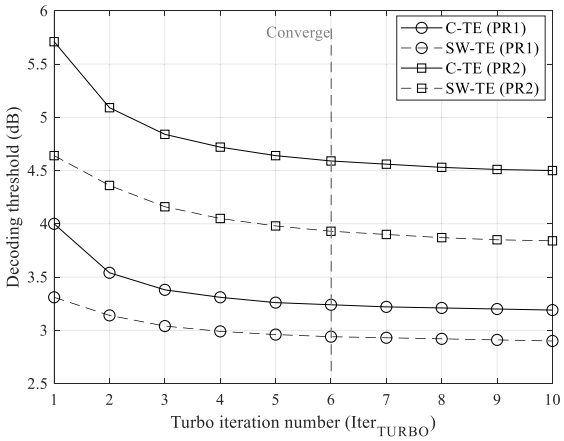

FIGURE 7. Relationship between decoding threshold and turbo iteration. The high-rate SC-LDPC codes are considered by $\mathbf{B}_{0,t} = \mathbf{B}_{1,t} = \mathbf{B}_{2,t} = [1\ 1\ 1\ 1\ 1]$.

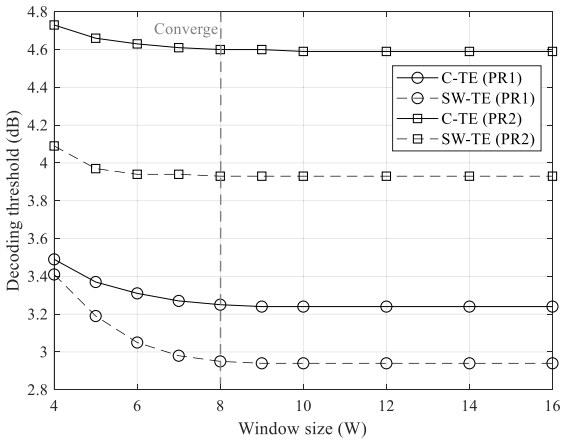

FIGURE 8. Relationship between decoding threshold and window size. The high-rate SC-LDPC codes are considered by $\mathbf{B}_{0,t} = \mathbf{B}_{1,t} = \mathbf{B}_{2,t} = [1\ 1\ 1\ 1\ 1]$.

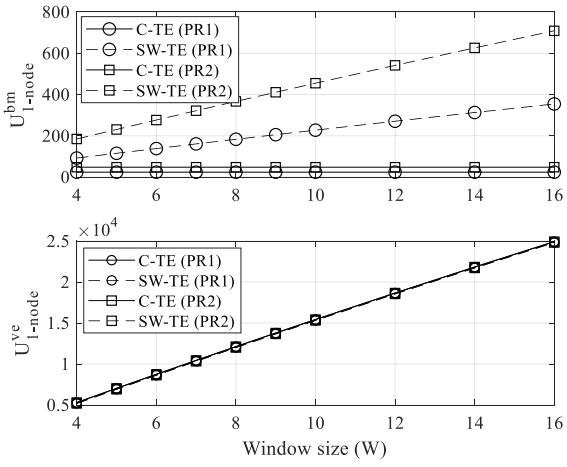

FIGURE 9. Number of updates of C-TE and SW-TE. The medium-rate SC-LDPC codes are considered by $\mathbf{B}_{0,t} = \mathbf{B}_{1,t} = \mathbf{B}_{2,t} = [1\ 1]$.

processing for the BCJR detector. When the window shifts to the next decoding position, $t = t + 1$, the BCJR detector

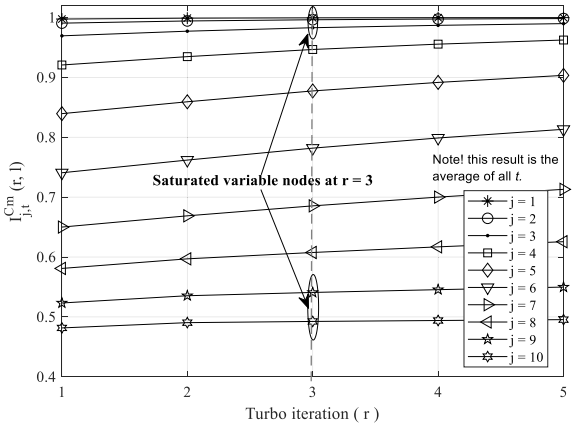

FIGURE 10. Mutual information improvements at the PR1 channel with $\mathbf{H}_{\mathbf{ISI}} = [1\ 1]$ and $E_b/N_0 = 1.1$ dB. The SC-LDPC codes are constructed with $\mathbf{B}_{0,t} = \mathbf{B}_{1,t} = \mathbf{B}_2 = [1\ 1]$. The value $W = 10$ and $Iter_{\mathbf{LDPC}} = 100$.

requires new priori information from the SC-LDPC decoder. Thus, the number of branch metric updates in SW-TE is higher than that of C-TE. As a result, although the SW-TE provides better decoding thresholds than the C-TE, $U^{\text{bm}}_{\text{1-node}}$ the SW-TE is significantly greater than the C-TE, especially for large W. Moreover, we observed that the SW-TE used in the PR2 channel always has larger $U^{\text{bm}}_{\text{1-node}}$ than the PR1 channel since they use a higher number of branch metrics.

Fig. 9 (lower) shows that $U^{\text{ve}}_{\text{1-node}}$ of C-TE and SW-TE are identical because they both use sliding-window processing for the SC-LDPC decoder.

V. REDUCED-COMPLEXITY DECODING TECHNIQUES FOR SW-TE

According to our analysis in Figs. 5 - 8, SW-TE provides better decoding thresholds than the C-TE for every $Iter_{\text{TURBO}}$ and W. However, a significant increase in branch metric updates, $U^{\text{bcjr}}_{\text{1-node}}$, is required in the BCJR detector, as shown in Fig. 9, particularly for large W and high interference effect (i.e., the PR2 channel). As a result, in the second half of this paper, we further propose a guideline of reduced-complexity decoding techniques for SW-TE, with the main goal of reducing $U^{\text{bm}}_{\text{1-node}}$.

A. IRREGULAR-UPDATING TECHNIQUE

During turbo iterative decoding, some variable nodes show no improvement in their soft information (i.e., LLR and mutual information) after the first few turbo iterations. For example, Fig. 10 shows the mutual information, $I^{Cm}_{j,t}(r, l)$ in (11), by ranging turbo iteration $r = 1$ to 5. We found that $I^{Cm}_{j,t}(r, l)$ improves by increasing r. However, some variable nodes such as $j = 1, 2, 3, 9$, and 10, show no significant $I^{Cm}_{j,t}(r, l)$ improvements after turbo iteration $r = 3$. Here, we refer to them as "*saturated variable nodes*." Saturation occurs because these nodes are sufficiently reliable. Thus, the decoding may not be required in the next iteration $r = 4$.

To reduce $U_{\text{1-node}}^{\text{bm}}$, we propose ignoring the branch metrics connected to the saturated variable nodes at the next turbo iteration. In this technique, we use $I_{j,t}^{Cm}(r,l)$ between turbo iteration r and $r-1$ to indicate the saturation behavior of variable nodes. Since $I_{j,t}^{Cm}(r,l)$ exists between 0 and 1, we compute $I_{j,t}^{Cm}(r,l)$ by taking $J^{-1}(\cdot)$. After decoding at turbo iteration, r, any variable nodes shown as

$$\frac{J^{-1}\left(I_{j,t}^{Cm}\left(r, Iter_{\text{LDPC}}\right)\right)}{J^{-1}\left(I_{j,t}^{Cm}\left(r-1, Iter_{\text{LDPC}}\right)\right)} \leq \beta_{\text{UB}}, \tag{12}$$

will be referred to as the saturated variable nodes. Thus, computations of the branch metrics associated with these saturated variable nodes will be ignored at the next turbo iteration $r+1$. The factor, β_{UB}, defines the upper bound indicating the saturated variable nodes. We select β_{UB} to obtain the minimum $U_{\text{1-node}}^{\text{bm}}$ while the decoding threshold is maintained (see the details in Section VI-A).

An example of the irregular updating technique is shown in Fig. 11. Assume that, after decoding at turbo iteration r, the saturated variable nodes exist at $j=1$ and 2, as shown in Fig. 11(a). As a result, the edges connecting these saturated variable nodes and the trellis nodes will be omitted at the next turbo iteration, $r+1$, as shown in Fig. 11(b). In addition, the branch metrics among the trellis nodes, $j=1$ to 2, will be omitted.

B. DYNAMIC-SHIFTING TECHNIQUE

One possibility for reducing the number of updates is to avoid unnecessary decoding positions, $2 \leq t \leq L$. In our previous work [23], the dynamic shifting of window decoding was introduced to reduce the complexity of the SC-LDPC decoder in the C-TE. This method could be applied straightforwardly to reduce the complexity of SW-TE. After decoding at position t, the window can be shifted to position $t+s$, where $1 \leq s \leq W$. Here, the number of position shifts, s, equals the number of variable nodes with approximately the same reliability as the 1st variable node (include the 1st variable node).

In this technique, unlike our previous work [23], we use mutual information, $I_{j,t}^{Cm}(r,l)$, to indicate the reliability of the variable nodes, j, at position t. The variable nodes, $2 \leq j \leq W$, are shown as

$$\frac{J^{-1}\left(I_{j,t}^{Cm}\left(Iter_{\text{TURBO}}, Iter_{\text{LDPC}}\right)\right)}{J^{-1}\left(I_{1,t}^{Cm}\left(Iter_{\text{TURBO}}, Iter_{\text{LDPC}}\right)\right)} \geq \alpha_{\text{LB}}, \tag{13}$$

which will be indicated as having the same level of reliability as the 1st variable node. Subsequently, they all become the output nodes of the window at position t. The factor, α_{LB}, defines the lower bound for indicating equivalent mutual information between the variable nodes, $2 \leq j \leq W$ and $j=1$.

As an example, if no variable nodes satisfy a condition in (13), the window will only shift one position to $t+1$ (or $s=1$), which is referred to as "*standard shifting*."

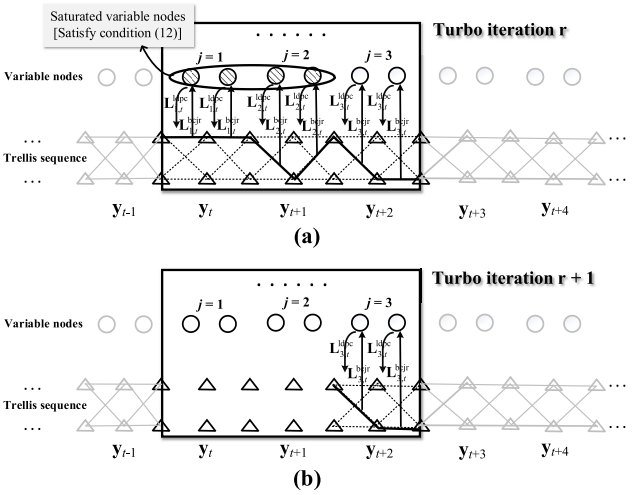

FIGURE 11. Example of the irregular-updating technique: (a) the saturated variable nodes $j=1$ and 2 exist at turbo iteration r, and therefore (b) the branch matric updates for $j=1$ and 2 are omitted at the next turbo iteration $r+1$.

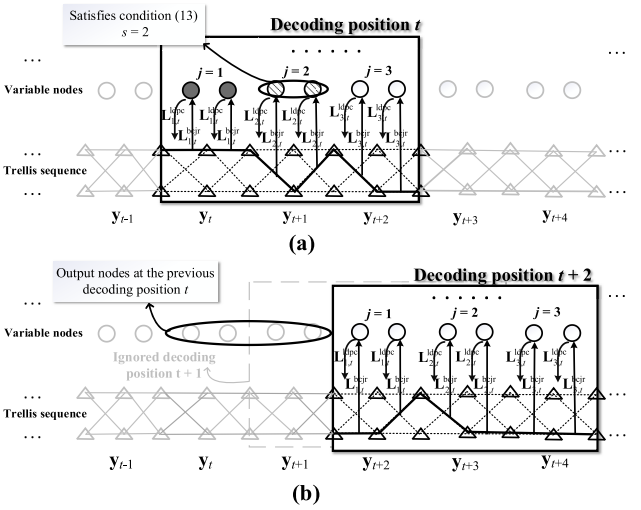

FIGURE 12. Example of dynamic shifting techniques: (a) the number of position shifts (s) is 2 at decoding position t, and therefore (b) the decoding at position $t+1$ is omitted, and the window is immediately shifted to position $t+2$.

If variable node $j=2$ satisfies (13), as seen in Fig. 12(a), the window will output two variable nodes, $j=1$ and 2 ($s=2$). Thus, we can ignore decoding at position, $t+1$, and shift the window to position $t+2$, as seen in Fig. 12(b).

C. COMBINED IRREGULAR-UPDATING AND DYNAMIC-SHIFTING TECHNIQUE

To further reduce $U_{\text{1-node}}^{\text{bm}}$, we combine the irregular-updating and dynamic-shifting techniques. According to our observations in the background, both techniques cannot be used together straightforwardly. In this technique, we propose an effective combination of both the irregular-updating and dynamic-shifting techniques as follows. If the window is shifted using the standard-shifting method ($s=1$), the irregular-updating technique will not be used at the next decoding position. This comes from the fact that,

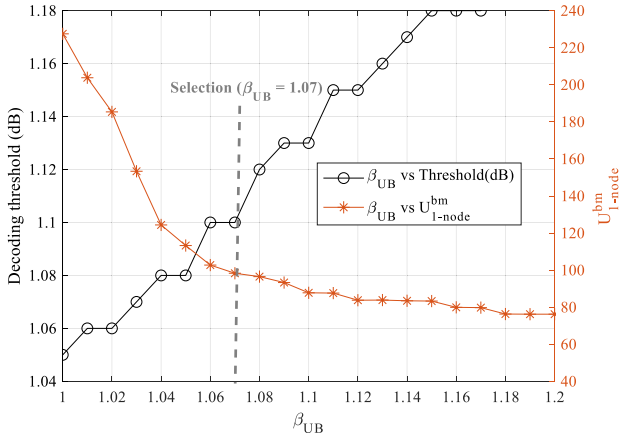

FIGURE 13. The decoding threshold and $U^{bm}_{1\text{-node}}$ of irregular updating technique for varied β_{UB}. The medium-rate SC-LDPC codes are considered by $\mathbf{B}_{0,t} = \mathbf{B}_{1,t} = \mathbf{B}_{2,t} = [1\ 1]$. The channel characteristic of PR1 channel is $\mathbf{H}_{ISI} = [1\ 1]$.

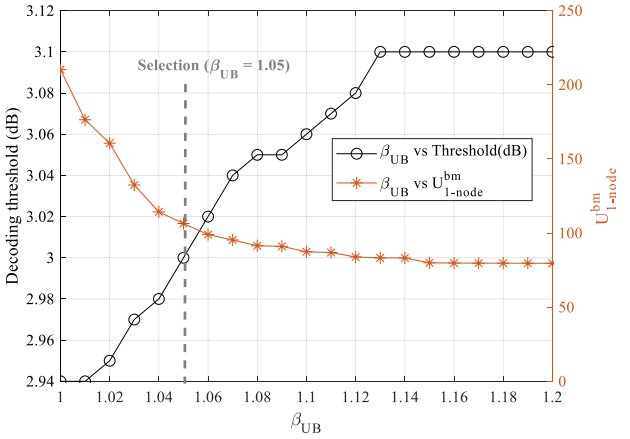

FIGURE 15. The decoding threshold and $U^{bm}_{1\text{-node}}$ of the irregular-updating technique for varied β_{UB}. The high-rate SC-LDPC codes are considered by $\mathbf{B}_{0,t} = \mathbf{B}_{1,t} = \mathbf{B}_{2,t} = [1\ 1\ 1\ 1\ 1]$. The channel characteristic of PR1 is $\mathbf{H}_{ISI} = [1\ 1]$.

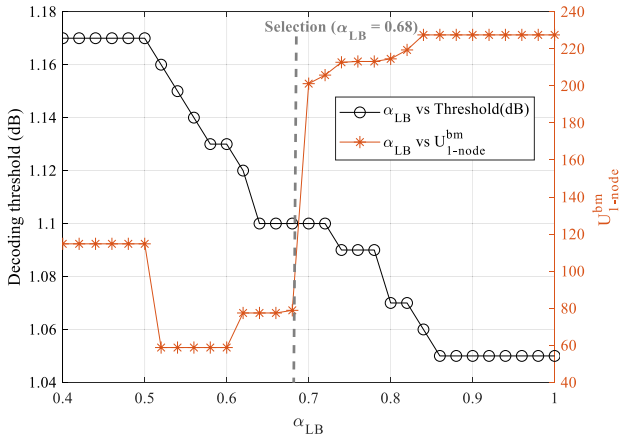

FIGURE 14. The decoding threshold and $U^{bm}_{1\text{-node}}$ of the dynamic shifting technique for varied α_{LB}. The medium-rate SC-LDPC codes are considered by $\mathbf{B}_{0,t} = \mathbf{B}_{1,t} = \mathbf{B}_{2,t} = [1\ 1]$. The channel characteristic of PR1 channel is $\mathbf{H}_{ISI} = [1\ 1]$.

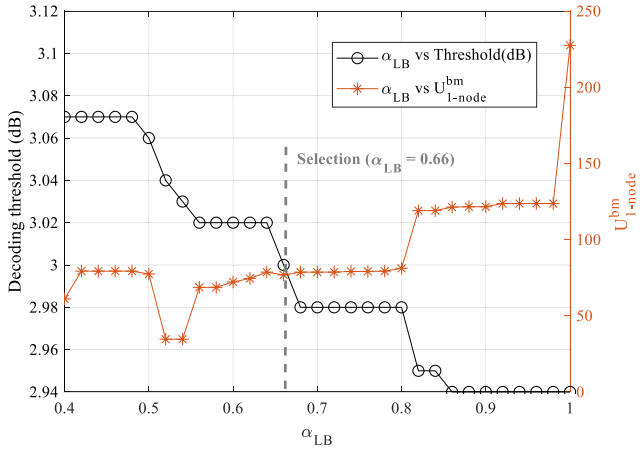

FIGURE 16. The decoding threshold and $U^{bm}_{1\text{-node}}$ of the dynamic shifting technique for varied α_{LB}. The high-rate SC-LDPC codes are considered by $\mathbf{B}_{0,t} = \mathbf{B}_{1,t} = \mathbf{B}_{2,t} = [1\ 1\ 1\ 1\ 1]$. The channel characteristic of PR1 is $\mathbf{H}_{ISI} = [1\ 1]$.

if the window is shifted in one position, the variable nodes, $2 \leq j \leq W$, can be viewed as low-reliability nodes. As a result, the irregular-updating technique should not be used in the next decoding position. On the other hand, the irregular-updating technique can be used at the next decoding position if the window is shifted in multiple positions ($s \geq 2$).

VI. INVESTIGATION OF OPTIMAL PARAMETERS AND PERFORMANCE EVALUATIONS VIA P-EXIT CHARTS

This section explains how to select the optimal β_{UB} for the irregular-updating technique and α_{LB} for the dynamic-shifting technique. Afterward, the complexity reductions of proposed techniques with β_{UB} and α_{LB} are presented. Keep in mind that our proposed techniques support all decoding parameters. However, only the complexity reductions of SW-TE with $W = 10$, $Iter_{TURBO} = 6$, and $Iter_{LDPC} = 100$ are presented in this paper.

A. OPTIMAL β_{UB} AND α_{LB} PARAMETERS

1) MEDIUM-RATE SC-LDPC CODES

In this part, we optimize β_{UB} by using the P-EXIT chart. The relationship between the decoding threshold and $U^{bm}_{1\text{-node}}$ for varied β_{UB} are shown in Fig. 13. The results show that we can reduce $U^{bm}_{1\text{-node}}$ more by increasing β_{UB}. However, the decoding thresholds will suffer. Thus, we select β_{UB} to obtain the minimum $U^{bcjr}_{1\text{-node}}$ without significant loss to the decoding threshold. For the PR1 channel, our selection is $\beta_{UB} = 1.07$, as seen by the grey-dotted line. Our selection for the PR2 channel is $\beta_{UB} = 1.06$ based on the same investigation, though it is not shown here.

To optimize α_{LB}, the decoding threshold and $U^{bm}_{1\text{-node}}$ are plotted by varying α_{LB}. The curves in Fig. 14 have the opposite trend as those in Fig. 13, in which we can reduce $U^{bm}_{1\text{-node}}$ more by decreasing α_{LB}. Our selection in the PR1 channel is $\alpha_{LB} = 0.68$, as seen on the grey-dotted line. Our selection

in the PR2 channel is $\alpha_{\mathrm{LB}} = 0.74$, though it is not shown here.

2) HIGH-RATE SC-LDPC CODES

In the case of SW-TE with high-rate SC-LDPC codes, the same optimization approaches are used. As seen in Fig. 15, our selection for the PR1 channel is $\beta_{\mathrm{UB}} = 1.05$. In the PR2 channel, our selection is $\beta_{\mathrm{UB}} = 1.04$ (not shown here). Fig. 16 shows that our selection for the PR1 channel is $\alpha_{\mathrm{LB}} = 0.66$. Furthermore, our selection for the PR2 channel is $\alpha_{\mathrm{LB}} = 0.78$ (not shown here).

B. ACHIEVEMENTS IN COMPLEXITY REDUCTION

1) MEDIUM-RATE SC-LDPC CODES

In this part, we compare $U^{\mathrm{bm}}_{\text{1-node}}$ ($U^{\mathrm{ve}}_{\text{1-node}}$) and decoding threshold for the C-TE and SW-TE. Table 1 lists $U^{\mathrm{bm}}_{\text{1-node}}$ ($U^{\mathrm{bm}}_{\text{1-node}}$) and decoding threshold when the medium-rate SC-LDPC code is used in C-TE and SW-TE. For the PR1 channel, the SW-TE has a lower (better) decoding threshold than the C-TE, but it requires many $U^{\mathrm{bm}}_{\text{1-node}} = 227.5$, whereas the C-TE only requires $U^{\mathrm{bm}}_{\text{1-node}} = 24$. Both the C-TE and SW-TE require identical $U^{\mathrm{bm}}_{\text{1-node}} = 15,317$. Our irregular-updating technique reduces $U^{\mathrm{bm}}_{\text{1-node}}$ of the SW-TE to 98.31 with only a 0.05 dB loss in the decoding threshold. Our dynamic-shifting technique reduces $U^{\mathrm{bm}}_{\text{1-node}}$ of the SW-TE to 78.89 and $U^{\mathrm{ve}}_{\text{1-node}}$ to 5,296 with the same decoding threshold loss. Unlike the irregular-updating technique, the dynamic-shifting technique can reduce both $U^{\mathrm{bm}}_{\text{1-node}}$ and $U^{\mathrm{ldpc}}_{\text{1-node}}$. Using a combination of the irregular-updating technique and dynamic-shifting technique, $U^{\mathrm{bm}}_{\text{1-node}}$ decreases to 51.54 and $U^{\mathrm{ve}}_{\text{1-node}}$ to 5,209, with a decoding threshold loss of 0.05 dB.

For the PR2 channel, $U^{\mathrm{bm}}_{\text{1-node}}$ ($U^{\mathrm{ve}}_{\text{1-node}}$) and the decoding threshold are listed in Table 1 as well. Similar to the case of the PR1 channel, the SW-TE has a lower (better) decoding threshold than the C-TE because it requires a much higher $U^{\mathrm{bm}}_{\text{1-node}} = 455$. Our irregular-updating technique reduces $U^{\mathrm{bm}}_{\text{1-node}}$ to 242.46 with decoding threshold losses of 0.06 dB. Our dynamic-shifting technique reduces $U^{\mathrm{bm}}_{\text{1-node}}$ to 201.54 and $U^{\mathrm{bm}}_{\text{1-node}}$ to 7,460, with a decoding threshold loss of 0.07 dB. When the irregular-updating and dynamic-shifting techniques are combined, $U^{\mathrm{bm}}_{\text{1-node}}$ decreases to 153.77 and $U^{\mathrm{ve}}_{\text{1-node}}$ to 7,615, with 0.08 dB threshold loss.

2) HIGH-RATE SC-LDPC CODES

Table 2 lists $U^{\mathrm{bm}}_{\text{1-node}}$ ($U^{\mathrm{ve}}_{\text{1-node}}$) and the decoding threshold of our proposed techniques when the C-TE and SW-TE use the high-rate SC-LDPC codes. For the PR1 channel, the SW-TE requires $U^{\mathrm{bm}}_{\text{1-node}} = 227.5$. Using the benefit of the irregular-updating technique, $U^{\mathrm{bm}}_{\text{1-node}}$ decreases to 106.47 with 0.06 dB loss in the decoding threshold. Our dynamic-shifting technique reduces $U^{\mathrm{bm}}_{\text{1-node}}$ to 76.81 with the same decoding threshold loss. Our combination technique reduces $U^{\mathrm{bm}}_{\text{1-node}}$ to 58.23 with a decoding threshold loss of 0.06 dB.

TABLE 1. Decoding thresholds and complexities of turbo equalizations. The medium-rate SC-LDPC codes are considered by $\mathbf{B}_{0,t} = \mathbf{B}_{1,t} = \mathbf{B}_{2,t} = [1\ 1]$.

Technique \ Output	Opt. parameter	Threshold (dB)	$U^{\mathrm{bm}}_{\text{1-node}}$	$U^{\mathrm{ve}}_{\text{1-node}}$
PR1 - $\mathbf{H}_{\mathrm{ISI}} = [1\ 1]$				
C-TE	N/A	1.48	24	15,317
SW-TE		1.05	227.5	15,317
SW-TE using **Irregular-updating**	$\beta_{\mathrm{UB}} = 1.07$	1.10	98.31	15,317
SW-TE using **Dynamic-shifting**	$\alpha_{\mathrm{LB}} = 0.68$	1.10	78.89	5,296
SW-TE using **Combination**	$\beta_{\mathrm{UB}} = 1.03$, $\alpha_{\mathrm{LB}} = 0.70$	1.10	51.54	5,209
PR2 - $\mathbf{H}_{\mathrm{ISI}} = [1\ 2\ 1]$				
C-TE	N/A	2.55	48	15,317
SW-TE		1.68	455	15,317
SW-TE using **Irregular-updating**	$\beta_{\mathrm{UB}} = 1.06$	1.74	242.46	15,317
SW-TE using **Dynamic-shifting**	$\alpha_{\mathrm{LB}} = 0.74$	1.75	201.54	7,460
SW-TE using **Combination**	$\beta_{\mathrm{UB}} = 1.03$, $\alpha_{\mathrm{LB}} = 0.76$	1.76	153.77	7,615

TABLE 2. Decoding thresholds and complexities of turbo equalizations. The high-rate SC-LDPC codes are considered by $\mathbf{B}_{0,t} = \mathbf{B}_{1,t} = \mathbf{B}_{2,t} = [1\ 1\ 1\ 1\ 1]$.

Technique \ Output	Opt. parameter	Threshold (dB)	$U^{\mathrm{bm}}_{\text{1-node}}$	$U^{\mathrm{ve}}_{\text{1-node}}$
PR1 - $\mathbf{H}_{\mathrm{ISI}} = [1\ 1]$				
C-TE	N/A	3.24	24	15,317
SW-TE		2.94	227.5	15,317
SW-TE using **Irregular-updating**	$\beta_{\mathrm{UB}} = 1.05$	3.00	106.47	15,317
SW-TE using **Dynamic-shifting**	$\alpha_{\mathrm{LB}} = 0.66$	3.00	76.81	5,158
SW-TE using **Combination**	$\beta_{\mathrm{UB}} = 1.05$, $\alpha_{\mathrm{LB}} = 0.79$	3.00	58.23	7,788
PR2 - $\mathbf{H}_{\mathrm{ISI}} = [1\ 2\ 1]$				
C-TE	N/A	4.59	48	15,317
SW-TE		3.93	455	15,317
SW-TE using **Irregular-updating**	$\beta_{\mathrm{UB}} = 1.04$	3.99	231.15	15,317
SW-TE using **Dynamic-shifting**	$\alpha_{\mathrm{LB}} = 0.78$	3.98	135.15	4,535
SW-TE using **Combination**	$\beta_{\mathrm{UB}} = 1.06$, $\alpha_{\mathrm{LB}} = 0.82$	3.99	126.30	7,909

For the PR2 channel, the SW-TE requires $U^{\mathrm{bm}}_{\text{1-node}} = 455$. $U^{\mathrm{bm}}_{\text{1-node}}$ decreases to 231.15 by using the irregular-updating technique, 135.15 by using the dynamic-shifting technique, and 126.30 by using the combination technique.

VII. COMPUTER-BASED SIMULATIONS

This section presents a computer-based simulation of the previous C-TE [23], [24] and our SW-TE. In our simulation, the parity-check matrix, $\mathbf{H}_t$, is constructed using a progressive edge-growth method [37] with an expansion factor of $N = 100$ for medium-rate and 40 for high-rate SC-LDPC codes. Hence, the total code word length for both the medium-rate and high-rate SC-LDPC codes is $n_{\rm V}LN = 20,000$ bits. In addition, the decoding parameters are set as follows: $W = 10$, $Iter_{\rm TURBO} = 6$, and $Iter_{\rm LDPC} = 10$.

A. BER ESTIMATIONS

In our three proposed techniques, we use mutual information from the P-EXIT chart to estimate how conditions (12) and (13) are activated or not activated. However, we must convert mutual information to a BER estimate for practical implementation. Following Hassan *et al.* [13], [18], we can estimate the BER of the variable node, j, after the turbo iteration, r,

$$\hat{P}_{j,t}(r) = \frac{1}{1+\exp\left(\left|\mathbf{L}_{j,t}^{\rm out}(r)\right|\right)}, \tag{14}$$

where $\mathbf{L}_{j,t}^{\rm out}(r)$ is the output LLR of the variable node. Thus, condition (12) can be rewritten as:

$$\frac{Q^{-1}\left(\hat{P}_{j,t}(r)\right)}{Q^{-1}\left(\hat{P}_{j,t}(r-1)\right)} \le \beta_{\rm UB}, \tag{15}$$

and condition (13) becomes,

$$\frac{Q^{-1}\left(\hat{P}_{j,t}(r)\right)}{Q^{-1}\left(\hat{P}_{1,t}(r)\right)} \ge \alpha_{\rm LB}, \tag{16}$$

where $Q^{-1}(\cdot)$ is the inverse Q-function.

B. BER AND COMPLEXITY COMPARISONS

1) MEDIUM-RATE SC-LDPC CODES

The simulation in Fig. 17 compares the BERs of C-TE and SW-TE when using medium-rate SC-LDPC codes. Starting with the PR1 channel, we found that the SW-TE surpasses the C-TE with a coding gain of about 0.22 dB at BER $= 4\times10^{-5}$. As seen in Fig. 18(a), this coding gain comes from the fact that the SW-TE uses a much higher $U_{\text{1-node}}^{\rm bm} = 227.5$, whereas the C-TE only requires $U_{\text{1-node}}^{\rm bm} = 24$. Our proposed techniques, including irregular-updating, dynamic-shifting, and their combination, can reduce $U_{\text{1-node}}^{\rm bm}$ of the SW-TE by more than a factor of two. In particular, the reductions in $U_{\text{1-node}}^{\rm bm}$ from our simulations converge to those of the P-EXIT chart analysis (i.e., Table 1). For example, the irregular-updating technique reduces $U_{\text{1-node}}^{\rm bm}$ to 100.12 at $\mathrm{E_b}/N_0 = 2.6$ dB. Our dynamic-shifting technique reduces $U_{\text{1-node}}^{\rm bm}$ to 80.65. The large reductions in $U_{\text{1-node}}^{\rm bm}$ are obtained by our combination technique, decreasing to 50.05. Note that all proposed techniques can reduce $U_{\text{1-node}}^{\rm bm}$ more than the previous BER-based dynamic-shifting technique [23], implying the advantage of the proposed algorithms based on tracking mutual information.

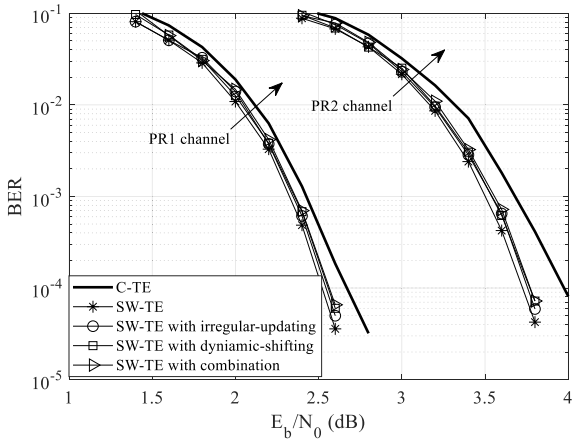

FIGURE 17. BER comparisons, where the medium-rate SC-LDPC codes are considered by $\mathbf{B}_{0,t} = \mathbf{B}_{1,t} = \mathbf{B}_{2,t} = [1\ 1]$.

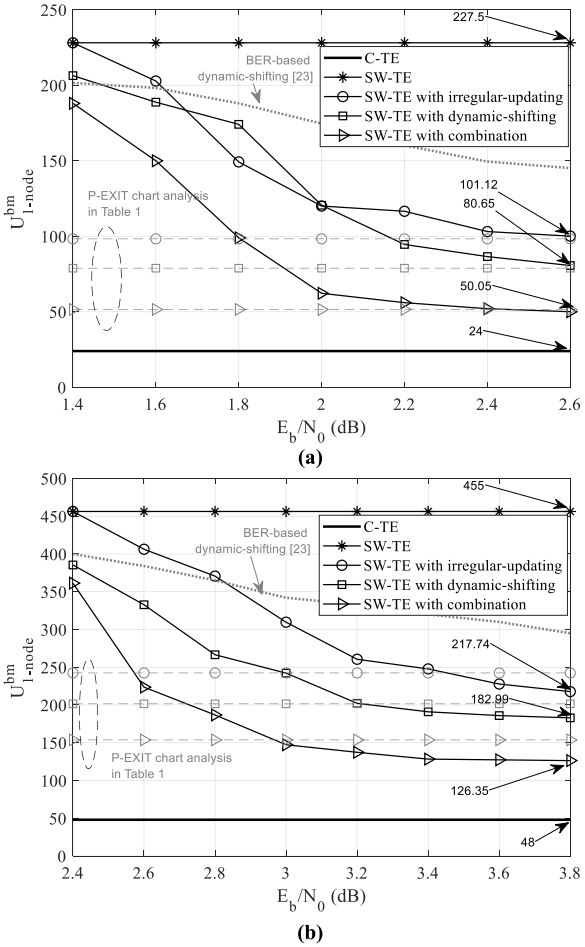

FIGURE 18. Comparison of $U_{\text{1-node}}^{\rm bcjr}$ in (a) PR1 and (b) PR2 channels, where the medium-rate SC-LDPC codes are considered by $\mathbf{B}_{0,t} = \mathbf{B}_{1,t} = \mathbf{B}_{2,t} = [1\ 1]$.

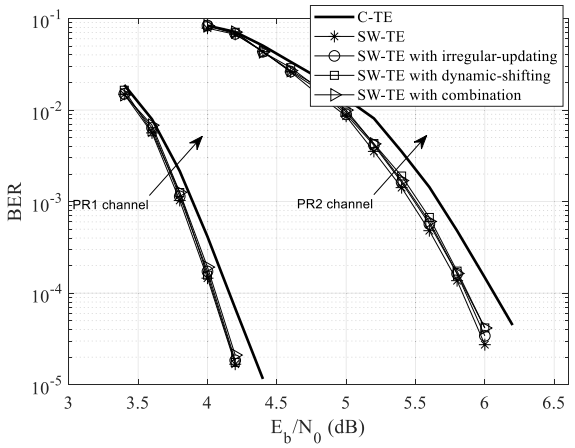

FIGURE 19. BER comparisons, where the high-rate SC-LDPC codes are considered by $\mathbf{B}_{0,t} = \mathbf{B}_{1,t} = \mathbf{B}_{2,t} = [1\ 1\ 1\ 1\ 1]$.

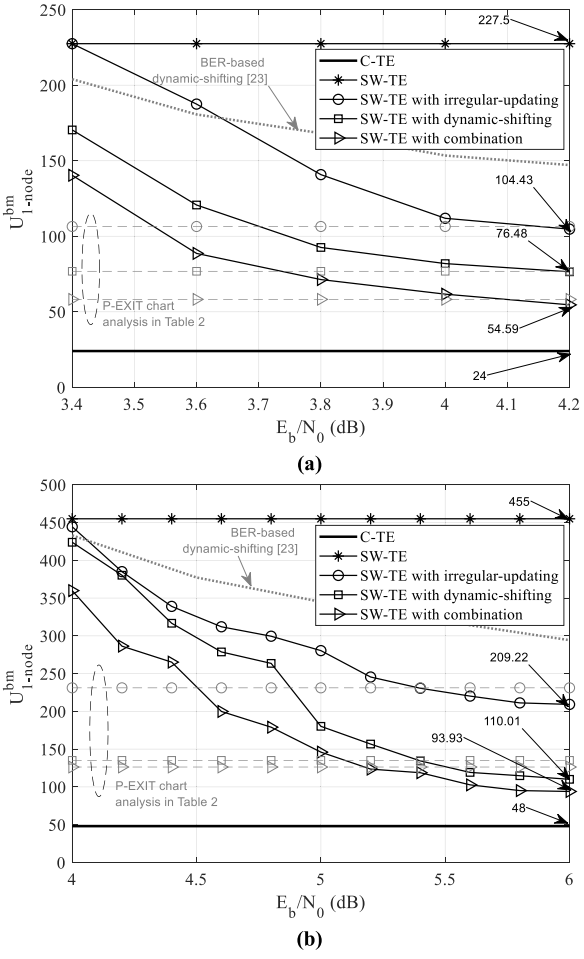

FIGURE 20. Comparison of $U^{\text{bcjr}}_{1\text{-node}}$ in (a) PR1 and (b) PR2 channels, where the high-rate SC-LDPC codes are considered by $\mathbf{B}_{0,t} = \mathbf{B}_{1,t} = \mathbf{B}_{2,t} = [1\ 1\ 1\ 1\ 1]$.

For the PR2 channel, the SW-TE outperforms the C-TE with a coding gain of about 0.27 dB at BER $= 4 \times 10^{-5}$. As seen in Fig. 18(b), the SW-TE requires a very high $U^{\text{bm}}_{1\text{-node}} = 455$, whereas the C-TE only requires $U^{\text{bm}}_{1\text{-node}} = 48$. We observed that the reductions of $U^{\text{bm}}_{1\text{-node}}$ from our simulations were slightly lower than those of the P-EXIT chart analysis. For example, our irregular-updating technique reduces $U^{\text{bm}}_{1\text{-node}}$ to 217.74 at $\mathrm{E_b}/N_0 = 3.8$ dB. Our dynamic-shifting technique reduces $U^{\text{bm}}_{1\text{-node}}$ to 182.99, while our combination technique reduces $U^{\text{bm}}_{1\text{-node}}$ to 126.35.

2) HIGH-RATE SC-LDPC CODES

A comparison of BERs when using high-rate SC-LDPC codes is shown in Fig. 19. The result shows that the SW-TE surpasses the C-TE for the PR1 channel with coding gains of 0.15 dB. The SW-TE requires $U^{\text{bm}}_{1\text{-node}} = 227.5$. The results in Fig. 20 show that the reductions in $U^{\text{bm}}_{1\text{-node}}$ from our simulations converge with those of the P-EXIT chart analysis (i.e., Table 2). At $E_b/N_0 = 4.2$ dB, $U^{\text{bm}}_{1\text{-node}}$ can be reduced to 104.43 by using our irregular-updating technique, 76.48 by using our dynamic-shifting technique, and 54.59 by using our combination technique.

For the PR2 channel, SW-TE requires $U^{\text{bm}}_{1\text{-node}} = 455$. $U^{\text{bm}}_{1\text{-node}}$ can be reduced to 209.22 when using our irregular-updating technique, 110.01 with our dynamic-shifting technique, and 93.93 with our combination technique.

VIII. CONCLUSION

In this paper, we propose "SW-TE," a new turbo equalization that uses sliding window decoding for both the BCJR detector and the SC-LDPC decoder. According to our P-EXIT chart analysis, the SW-TE has a better decoding threshold than the C-TE, at the cost of much higher computational complexity in terms of $U^{\text{bm}}_{1\text{-node}}$. As a result, we further propose a guideline of reduced-complexity decoding techniques for SW-TE: 1) irregular-updating, 2) dynamic-shifting, and 3) their combination. Our simulations confirm our analyses, showing that our proposed techniques reduce $U^{\text{bm}}_{1\text{-node}}$ of the SW-TE by more than a factor of two without significant loss in BERs. For example, the SW-TE outperforms the C-TE with a coding gain of 0.25 dB in high-rate SC-LDPC codes and the PR2 channel, but it requires an extremely high $U^{\text{bm}}_{1\text{-node}} = 455$. For the reduced-complexity SW-TE, $U^{\text{bm}}_{1\text{-node}}$ decreases to 209.22 (∼54%) using the irregular-updating technique, 110.01 (∼76%) using the dynamic-shifting technique, and 93.93 (∼80%) using the combination technique.

REFERENCES

[1] C. Gong and Z. Xu, "Channel estimation and signal detection for optical wireless scattering communication with inter-symbol interference," *IEEE Trans. Wireless Commun.*, vol. 14, no. 10, pp. 5326–5337, Oct. 2015.

[2] E. Hwang, R. Negi, and B. V. K. V. Kumar, "Signal processing for near 10 Tbit/in^2 density in two-dimensional magnetic recording (TDMR)," *IEEE Trans. Magn.*, vol. 46, no. 6, pp. 1813–1816, Jun. 2010.

[3] C. Douillard, M. Jézéquel, C. Berrou, A. Picart, P. Didier, and A. Glavieux, "Iterative correction of intersymbol interference: Turbo-equalization," *Eur. Trans. Telecommun.*, vol. 6, no. 5, pp. 507–511, 1995.

[4] M. Tuchler, R. Koetter, and A. C. Singer, "Turbo equalization: Principles and new results," *IEEE Trans. Commun.*, vol. 50, no. 5, pp. 754–767, May 2002.

[5] H. Alhussien, J. Park, and J. Moon, "Iterative decoding based on error pattern correction," *IEEE Trans. Magn.*, vol. 44, no. 1, pp. 181–186, Jan. 2008.

[6] F. Sun and T. Zhang, "Quasi-reduced-state soft-output Viterbi detector for magnetic recording read channel," *IEEE Trans. Magn.*, vol. 43, no. 10, pp. 3921–3924, Oct. 2007.
[7] H. Song and B. V. K. V. Kumar, "Low-density parity-check codes for partial response channels," *IEEE Signal Process. Mag.*, vol. 21, no. 1, pp. 56–66, Jan. 2004.
[8] M. Sabbaghian and D. Falconer, "Comparison between convolutional and LDPC code-based turbo frequency domain equalization," in *Proc. IEEE Int. Conf. Commun.*, Jun. 2006, pp. 5432–5437.
[9] Y. Fang, G. Han, G. Cai, F. C. M. Lau, P. Chen, and Y. L. Guan, "Design guidelines of low-density parity-check codes for magnetic recording systems," *IEEE Commun. Surveys Tuts.*, vol. 20, no. 2, pp. 1574–1606, 2nd Quart., 2018.
[10] A. J. Felstrom and K. S. Zigangirov, "Time-varying periodic convolutional codes with low-density parity-check matrix," *IEEE Trans. Inf. Theory*, vol. 45, no. 6, pp. 2181–2191, Sep. 1999.
[11] S. Kudekar, T. J. Richardson, and R. L. Urbanke, "Threshold saturation via spatial coupling: Why convolutional LDPC ensembles perform so well over the BEC," *IEEE Trans. Inf. Theory*, vol. 57, no. 2, pp. 803–834, Feb. 2011.
[12] A. E. Pusane, R. Smarandache, P. O. Vontobel, and D. J. Costello, "Deriving good LDPC convolutional codes from LDPC block codes," *IEEE Trans. Inf. Theory*, vol. 57, no. 2, pp. 835–857, Feb. 2011.
[13] N. Ul Hassan, M. Lentmaier, and G. P. Fettweis, "Comparison of LDPC block and LDPC convolutional codes based on their decoding latency," in *Proc. 7th Int. Symp. Turbo Codes Iterative Inf. Process. (ISTC)*, Aug. 2012, pp. 225–229.
[14] F. R. Kschischang, B. J. Frey, and H.-A. Loeliger, "Factor graphs and the sum-product algorithm," *IEEE Trans. Inf. Theory*, vol. 47, no. 2, pp. 498–519, Feb. 2001.
[15] A. R. Iyengar, M. Papaleo, P. H. Siegel, J. K. Wolf, A. Vanelli-Coralli, and G. E. Corazza, "Windowed decoding of protograph-based LDPC convolutional codes over erasure channels," *IEEE Trans. Inf. Theory*, vol. 58, no. 4, pp. 2303–2320, Apr. 2012.
[16] I. Ali, J.-H. Kim, S.-H. Kim, H. Kwak, and J.-S. No, "Improving windowed decoding of SC LDPC codes by effective decoding termination, message reuse, and amplification," *IEEE Access*, vol. 6, pp. 9336–9346, 2018.
[17] K. Klaiber, S. Cammerer, L. Schmalen, and S. T. Brink, "Avoiding burst-like error patterns in windowed decoding of spatially coupled LDPC codes," in *Proc. IEEE 10th Int. Symp. Turbo Codes Iterative Inf. Process. (ISTC)*, Hong Kong, Dec. 2018, pp. 1–5.
[18] N. U. Hassan, A. E. Pusane, M. Lentmaier, G. P. Fettweis, and D. J. Costello, "Non-uniform window decoding schedules for spatially coupled LDPC codes," *IEEE Trans. Commun.*, vol. 65, no. 2, pp. 501–510, Feb. 2017.
[19] H. Esfahanizadeh, A. Hareedy, and L. Dolecek, "Spatially coupled codes optimized for magnetic recording applications," *IEEE Trans. Magn.*, vol. 53, no. 2, pp. 1–11, Feb. 2017.
[20] Z. Yang, Y. Fang, G. Zhang, G. Han, and L. Kong, "Performance analysis and optimization of spatially coupled protograph-based low-density parity-check codes for two-dimensional magnetic recording systems," *IEEE Trans. Magn.*, vol. 56, no. 3, pp. 1–7, Mar. 2020.
[21] A. Hareedy, R. Wu, and L. Dolecek, "A channel-aware combinatorial approach to design high performance spatially-coupled codes," *IEEE Trans. Inf. Theory*, vol. 66, no. 8, pp. 4834–4852, Aug. 2020.
[22] A. Hareedy, R. Kuditipudi, and R. Calderbank, "Minimizing the number of detrimental objects in multi-dimensional graph-based codes," *IEEE Trans. Commun.*, vol. 68, no. 9, pp. 5299–5312, Sep. 2020.
[23] S. Khittiwitchayakul, W. Phakphisut, and P. Supnithi, "Reduced complexity window decoding of spatially coupled LDPC codes for magnetic recording systems," *IEEE Trans. Magn.*, vol. 54, no. 11, pp. 1–5, Nov. 2018.
[24] S. Khittiwitchayakul, W. Phakphisut, and P. Supnithi, "Associated sectors of magnetic recording systems using spatially coupled LDPC codes," *ECTI Trans. Electr. Eng., Electron., Commun.*, vol. 20, no. 1, pp. 10–21, Feb. 2022.
[25] L. Bahl, J. Cocke, F. Jelinek, and J. Raviv, "Optimal decoding of linear codes for minimizing symbol error rate (corresp.)," *IEEE Trans. Inf. Theory*, vol. IT-20, no. 2, pp. 284–287, Mar. 1974.
[26] S. Khittiwitchayakul, W. Phakphisut, and P. Supnithi, "Sliding-window processing of turbo equalization for partial response channels," in *Proc. 26th Int. Conf. Telecommun. (ICT)*, Apr. 2019, pp. 182–186.
[27] G. Liva and M. Chiani, "Protograph LDPC codes design based on EXIT analysis," in *Proc. IEEE Global Telecommun. Conf. (GLOBECOM)*, Nov. 2007, pp. 3250–3254.
[28] J. Thorpe, "Low-density parity-check (LDPC) codes constructed from protographs," JPL, Pasadena, CA, USA, Tech. Rep. 154, 2003.
[29] D. G. M. Mitchell, M. Lentmaier, and D. J. Costello, "Spatially coupled LDPC codes constructed from protographs," *IEEE Trans. Inf. Theory*, vol. 61, no. 9, pp. 4866–4889, Sep. 2015.
[30] R. M. Tanner, D. Sridhara, A. Sridharan, T. E. Fuja, and D. J. Costello, "LDPC block and convolutional codes based on circulant matrices," *IEEE Trans. Inf. Theory*, vol. 50, no. 12, pp. 2966–2984, Dec. 2004.
[31] J. Gwak, S. K. Shin, and H. M. Kim, "Reduced complexity sliding window BCJR decoding algorithms for turbo codes," in *Cryptography and Coding*, M. Walker, Ed. Cham, Switzerland: Springer, 1999, pp. 179–184, doi: 10.1007/3-540-46665-7_20.
[32] M. Lentmaier, M. M. Prenda, and G. P. Fettweis, "Efficient message passing scheduling for terminated LDPC convolutional codes," in *Proc. IEEE Int. Symp. Inf. Theory Proc.*, Jul. 2011, pp. 1826–1830.
[33] A. J. Viterbi, "An intuitive justification and a simplified implementation of the MAP decoder for convolutional codes," *IEEE J. Sel. Areas Commun.*, vol. 16, no. 2, pp. 260–264, Feb. 1998.
[34] D. J. Costello, A. Pusane, S. Bates, and K. S. Zigangirov, "A comparison between LDPC block and convolutional codes," in *Proc. Inform. Theory App. Workshop*, San Diego, CA, USA, Feb. 2006, pp. 6–10.
[35] T. Van Nguyen, A. Nosratinia, and D. Divsalar, "Protograph-based LDPC codes for partial response channels," in *Proc. IEEE Int. Conf. Commun. (ICC)*, Ottawa, ON, Canada, Jun. 2012, pp. 2166–2170.
[36] S. ten Brink, G. Kramer, and A. Ashikhmin, "Design of low-density parity-check codes for modulation and detection," *IEEE Trans. Commun.*, vol. 52, no. 4, pp. 670–678, Apr. 2004.
[37] X.-Y. Hu, E. Eleftheriou, and D. M. Arnold, "Regular and irregular progressive edge-growth tanner graphs," *IEEE Trans. Inf. Theory*, vol. 51, no. 1, pp. 386–398, Jan. 2005.

SIRAWIT KHITTIWITCHAYAKUL received the B.Eng. and M.Eng. degrees in telecommunication engineering and the D.Eng. degree in electrical engineering from the King Mongkut's Institute of Technology Ladkrabang, Bangkok, Thailand, in 2014, 2017, and 2022, respectively. His main research interest includes error correction codes for magnetic recording systems.

WATID PHAKPHISUT (Member, IEEE) received the B.Eng. degree in telecommunication engineering, the M.Eng. degree in data storage technology, and the D.Eng. degree in electrical engineering from the King Mongkut's Institute of Technology Ladkrabang, Bangkok, Thailand, in 2009, 2011, and 2015, respectively. His research interests include error correction codes, and artificial intelligence for communication and data storage systems.